JOURNAL OF AIRCRAFT
Vol. 37, No. 3, May–June 2000

Computational Study of Flapping Airfoil Aerodynamics

Ismail H. Tuncer*
Middle East Technical University, 06531 Ankara, Turkey
and
Max F. Platzer†
Naval Postgraduate School, Monterey, California 93943

Unsteady, viscous, low-speed flows over a NACA 0012 airfoil oscillated in plunge and/or pitch at various reduced frequency, amplitude, and phase shift are computed. Vortical wake formations, boundary-layer flows at the leading edge, the formation of leading-edge vortices and their downstream convection are presented in terms of unsteady particle traces. Flow separation characteristics and thrust-producing wake profiles are identified. Computed results compare well with water tunnel flow visualization and force data and other computational data. The maximum propulsive efficiency is obtained for cases where the flow remains mostly attached over the airfoil oscillated in a combined pitch and plunge.

Nomenclature

$\bar{C}_D$ = time-averaged drag (thrust) coefficient, $\bar{D}/\frac{1}{2}\rho U_\infty^2 c$
c = airfoil chord length (reference length)
h = plunge position normalized with c
h_0 = plunge amplitude normalized with c
k = reduced frequency ($\omega c/U_\infty$)
t = nondimensional time
U_∞ = freestream velocity (reference speed)
α = incidence angle
α_0 = pitch amplitude
η = propulsive efficiency
ϕ = phase shift between pitch and plunge oscillations
ω = angular frequency of oscillation

Introduction

THE separated flows over helicopter, propeller, and wind turbine blades have received considerable attention for quite some time because of the impact of dynamic stall on the blade performance. In recent years a significant amount of new experimental information has been obtained. For a comprehensive review of this experimental data, we refer to the review paper by Carr and Chandrasekhara.[1] Also, the rapid advances in computational fluid dynamics have made it possible to apply numerical solution techniques of the Reynolds-averaged Navier–Stokes equations to this problem. Recent contributions to this problem have been reviewed by Ekaterinaris and Platzer,[2] who also showed that the incorporation of the boundary-layer transition from laminar to turbulent flow into the Navier–Stokes code provides much better agreement with the measurements.

The case of sinusoidal plunge oscillations has received much less attention in past years because a pure plunge oscillation was thought to have much less importance in practical applications. However, it has been known for many years that a sinusoidally plunging wing generates a thrust force. This effect can be predicted using inviscid incompressible flow theory. For example, Garrick[3] used Theodorsen's oscillatory thin-airfoil theory, and Platzer et al.[4] applied an unsteady panel code to this problem.

Very recently, it has been recognized that flapping wing propulsion can be more efficient than conventional propellers if applied to very small-scale vehicles, so-called microair vehicles, because of the very small Reynolds numbers encountered on such vehicles. The word *flapping* is used to indicate a combined plunge-and-pitch oscillation. Of special interest is the determination of the dependence of the thrust force on the amplitude, frequency, and phase angle between plunge-and-pitch oscillation and on the flow Reynolds number, especially the combination of these parameters, which leads to dynamic stall and therefore loss of thrust and propulsive efficiency.

Water-tunnel flow-visualization experiments have been conducted by Jones et al.[5] and Lai and Platzer,[6] which provide a considerable amount of information on the wake characteristics generated by flapping airfoils. An example of such a visualization is given in Fig. 1. Also, Navier–Stokes computations have been performed by Tuncer and colleagues[7–9] to explore the thrust generation and propulsive efficiency of flapping airfoils. The only other Navier–Stokes analyses of flapping and pitching airfoils are those of Isogai et al.[10] and of Ramamurti et al.[11] Isogai et al.[10] found for the NACA 0012 airfoil that at a Reynolds number 1×10^5 the highest efficiency occurs when the pitch oscillation leads the plunge oscillation by 90 deg while flow separation is still confined to a small region near the trailing edge. Ramamurti et al.[11] also studied the NACA 0012 airfoil, but at much lower Reynolds numbers of 1.2×10^4 and 1.1×10^3 using an incompressible Navier–Stokes solver.

The objective of the present work is to compute unsteady, viscous flowfields over a flapping NACA 0012 airfoil at various reduced frequencies and amplitudes and to identify the vortical wake and the stall characteristics. To this end, a Navier–Stokes solver augmented with a particle tracing module is employed to compute the unsteady flowfields. The flow separation characteristics over the airfoil, vortical wake formations, average aerodynamic forces, and the propulsive efficiency are studied parametrically with respect to the amplitude and the frequency of the oscillatory motion. Numerical predictions are compared to the water-tunnel flow-visualization data,[6] force and power data,[12] and the recent computations of Isogai et al.[10]

Numerical Method

The steady and unsteady flowfields over a flapping airfoil are computed by a compressible Navier–Stokes solver at a low subsonic Mach number. The computed flowfields are analyzed in terms of particle traces emanating from the leading and trailing edges of the airfoil and the time-averaged aerodynamic loads.

Navier–Stokes Solver

The strong conservation-law form of the two-dimensional, thin-layer, Reynolds-averaged, compressible Navier–Stokes equations

Received 8 June 1999; revision received 19 November 1999; accepted for publication 12 December 1999. This material is declared a work of the U.S. Government and is not subject to copyright protection in the United States.

*Associate Professor, Department of Aeronautical Engineering; tuncer@ae.metu.edu.tr. Member AIAA.
†Distinguished Professor, Department of Aero/Astronautics; platzer@aa.nps.navy.mil. Fellow AIAA.

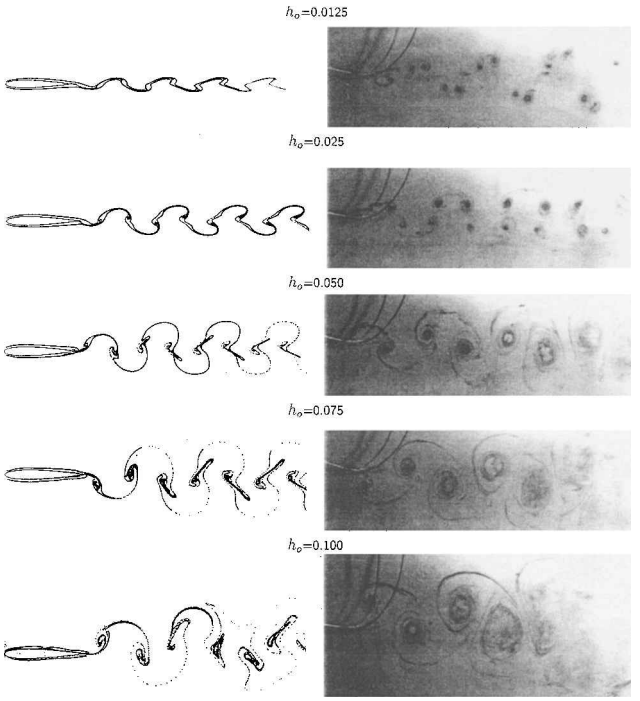

Fig. 1 Unsteady particle traces vs flow-visualization data behind a NACA 0012 airfoil oscillated in plunge at k = 7.85.

is solved using an approximately factored, implicit algorithm.[2,7] The convective terms are evaluated using the third-order-accurate Osher's upwind-biased flux-difference-splitting scheme.[13] The governing equations in a curvilinear coordinate system (ξ, ζ) are given as follows:

$$\partial_t \hat{\boldsymbol{Q}} + \partial_\xi \hat{\boldsymbol{F}} + \partial_\zeta \hat{\boldsymbol{G}} = Re^{-1} \partial_\zeta \hat{\boldsymbol{S}} \tag{1}$$

where $\hat{\boldsymbol{Q}}$ is the vector of conservative variables, $1/J(\rho, \rho u, \rho w, e)$, $\hat{\boldsymbol{F}}$ and $\hat{\boldsymbol{G}}$ are the inviscid flux vectors, and $\hat{\boldsymbol{S}}$ is the thin-layer approximation of the viscous fluxes in the ζ direction normal to the airfoil surface. The pressure is related to density and total energy through the equation of state for an ideal gas $p = (\gamma - 1)[e - \rho(u^2 + w^2)/2]$. In turbulent flow computations the Baldwin–Lomax turbulence model is implemented.

Computational Domain

The computational domain around the airfoil is discretized with a single C grid. The flapping motion of the airfoil is imposed by moving the airfoil and the computational grid as specified by the oscillatory motion:

$$h = -h_0 \cos(kt) \qquad \alpha = -\alpha_0 \cos(kt + \phi) \tag{2}$$

where h_0 is the plunge amplitude (normalized with the airfoil chord), α_0 denotes the pitch amplitude, and ϕ is the leading phase angle between the pitching and plunging motion. The reduced frequency of the motion is defined by $k = \omega c / U_\infty$.

Boundary Conditions

On the airfoil surface the instantaneous flow velocity is set equal to the prescribed local surface velocity prescribed by the oscillatory motion [Eq. (2)], and the no-slip boundary condition is applied. The density and the pressure gradients are also set to zero. At the far-field inflow and outflow boundaries the flow variables are evaluated using the zeroth-order Riemann invariant extrapolation.

Particle Traces

Localization Process

Particle traces are obtained by a simple and efficient integration of particle pathlines within the flow solver as the unsteady flowfield is computed. In this method particles may be released anywhere in the flowfield at certain intervals. The particles are then localized in the computational grid and convected with the local velocity at every particle path-integration time step. The localization process is based on a directional and a sequential search algorithm.[14] The search process follows a deterministic path, which is based on the local geometry gradients on the curvilinear grid. A particle is localized in a triangular stencil identified by three neighboring grid points. The localization scheme also provides the interpolation weights at the localization point in terms of function values at the corner points of the localizing triangular stencil. Therefore, once a particle is localized in the computational grid, the local velocity is readily interpolated at the localization point and can be used for convecting the particle.

Numerical Implementation

The particle localization and velocity interpolation algorithm is implemented into the Navier–Stokes solver as a function call. The function shares only the grid geometry and flow variables at the current time step with the solver. The particles can be released from any grid location at any given frequency in terms of the timescale of the unsteady motion. A simple algorithm is also implemented to identify the presence of wake cuts in C-type grids. Particles can therefore be convected across the wake cuts without any difficulty.

Because the accuracy of the particle traces depends on the size of the integration time step, a higher resolution of the timescale allows particles to follow closely the local velocity field and mostly prevents them from penetrating into solid surfaces on their path. However, at high-frequency motions particles in the close vicinity of the airfoil surface can be wrongfully placed inside the airfoil because of grid movement. These particles stuck inside the airfoil are convected out of the airfoil with the freestream velocity. Although the time integration of particle paths can be performed at every time step of the flow solver, the time step of pathline integration was found to be one order of magnitude larger than the time-step size of the unsteady flow solver. Yet, it is controlled by the user. The instantaneous positions of all of the particles can be saved at any frequency for visualization purposes.

Results and Discussion

In our earlier flow-visualization studies we have identified the thrust-producing wake structures behind an airfoil oscillated in plunge as the lower row of vortices are rotating clockwise while the upper row of vortices are rotating counterclockwise. We have also observed that airfoils which undergo thrust-producing combined pitch-and-plunge oscillations do not, in general, go through a distinct dynamic stall loop. In this study we have looked at the unsteady flowfields behind oscillating airfoils in pitch and plunge in terms of particle traces and compared the computed flowfields to the available experimental data.

All of the flowfields were computed for a NACA 0012 airfoil at a low freestream Mach number of 0.3. The flowfields were assumed to be fully turbulent. Based on our earlier grid-sensitivity study,[9] where we showed that the computed results were not sensitive to the finer grid size, we used a 121×61 size C-type grid in all of the computations. Particles were shed from the two neighboring grid points in the crossflow direction on the upper and lower surfaces around the leading and trailing edges. Particles were shed at about every $0.01\ c/U_\infty$ (chord length travel) time.

We first computed unsteady flowfields over a plunging airfoil at a reduced frequency of $k = 7.85$, $Re = 2 \times 10^4$ for $h_0 = 0.0125$, 0.025, 0.05, 0.075, and 0.1. The comparison of the wake profiles with the experimental data[6] is given in Fig. 1. The experiments were also performed at about $Re = 2 \times 10^4$, and the dye was ejected from the trailing edge of the airfoil to facilitate wake visualization.

Lai and Platzer[6] noted that a jet and hence thrust is produced as soon as the nondimensional plunge velocity kh_0 exceeds values greater than approximately 0.2. As seen from Table 1, this agrees quite well with the computed thrust values. For $h_0 = 0.025$ and $k = 7.85$ the value of $kh_0 = 0.2$ and, in agreement with the experiment, a tiny amount of thrust is predicted, whereas for $h_0 = 0.0125$

Table 1 Thrust of NACA 0012 airfoil oscillated in plunge

$k = 7.85$	
h_0	$\bar{C}_D$
0.0125	0.008
0.0250	−0.004
0.0500	−0.045
0.0750	−0.101
0.1000	−0.176

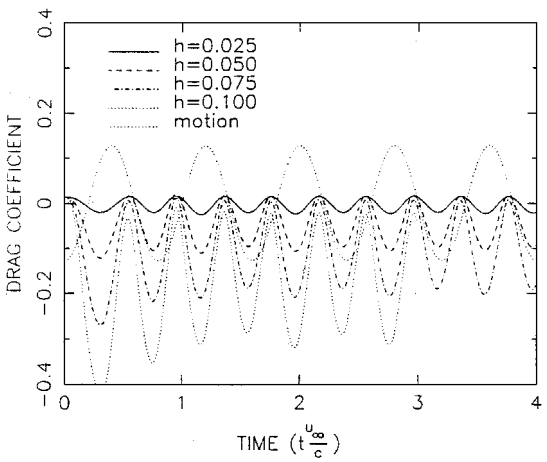

Fig. 2 Time history of drag coefficient for a NACA 0012 airfoil oscillated in plunge at $k = 7.85$.

and $k = 7.85$, corresponding to $kh_0 = 0.1$, and again consistent with the experiment, drag is predicted. The computed vortex patterns for $kh_0 = 0.1$ and 0.2 are in poor agreement with the observed vortices. This discrepancy is likely caused by viscous effects that are stronger at low nondimensional plunge velocities, but further work is required to clarify this conjecture. For thrust-producing vortex streets $kh_0 = 0.4, 0.59, 0.78$; the agreement is quite good. The upper-row vortices are counterclockwise and the lower vortices clockwise. This is the condition for producing a jet flow in contrast to the drag-producing Karman vortex street shed from a stationary cylinder, where the upper vortices are clockwise and the lower vortices are counterclockwise.

Figure 2 gives the unsteady thrust/drag history. The average drag coefficients per cycle computed at the last period are also given in Table 1. As seen, as the plunge amplitude h_0 increases, the airfoil experiences higher thrust for longer durations along each plunging cycle. Starting from $h_0 = 0.025$, where the counterclockwise and clockwise vortices were observed to be positioned below and above the wake centerline (Fig. 1), respectively, the flapping airfoil produces a net thrust.

The instantaneous flowfield at about $h = 0.0 \downarrow$ for $k = 7.85$ case is given in Fig. 3 in terms of Mach number and vorticity contours and particle traces. As seen, the integrated effect of the vorticity in the formation of wake profiles is only captured in the particle traces. It can, therefore, be misleading to compare instantaneous Mach number and vorticity distributions to flow-visualization data.

Next we looked at the flow separation characteristics of high-amplitude/low-frequency plunging airfoils at $k = 0.8$, $Re = 1 \times 10^5$ as the plunge amplitude changes from 0.4 to 0.7. Figures 4a–4d show the computed flowfields. At $h_0 = 0.40$ the flow is fully attached all along the plunging motion, which gives the largest propulsive efficiency of 0.59 as given in Table 2. The propulsive efficiency is defined as

$$\eta = -\bar{C}_D \cdot U_\infty / \bar{W}$$

where $\bar{W}$ is the average work required to maintain the flapping motion, which is computed by integrating the pressure distribution times the local plunge velocity on the airfoil. The time averaging is done over a period of the oscillatory motion.

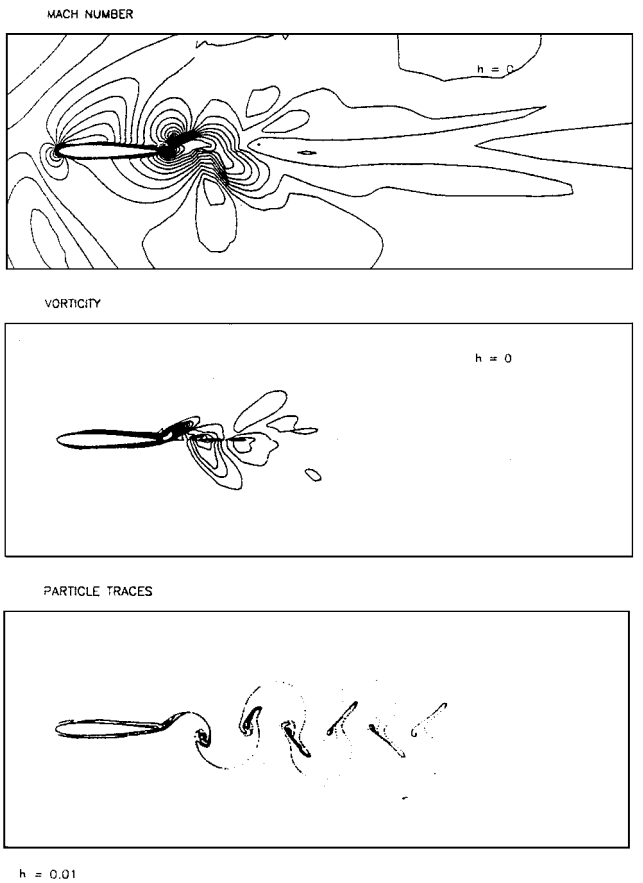

Fig. 3 Instantaneous flowfield behind a NACA 0012 airfoil oscillated in plunge at $k = 7.85$ and $h_0 = 0.075$.

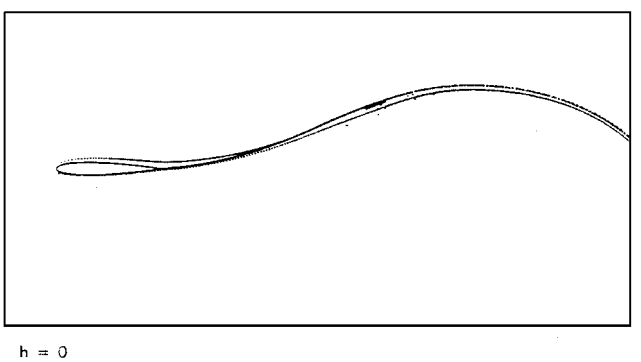

Fig. 4a Unsteady particle traces over a NACA 0012 airfoil oscillated in plunge at $k = 0.8$ and $h_0 = 0.40$.

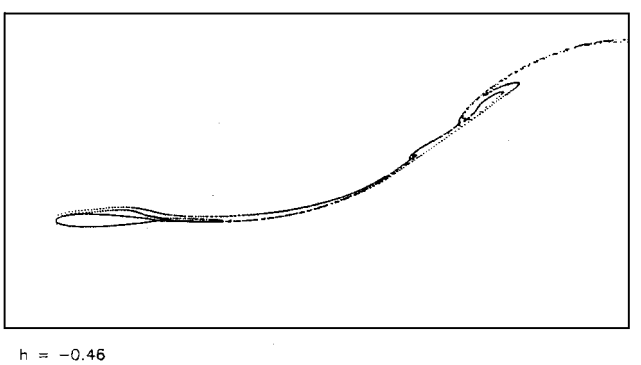

Fig. 4b Unsteady particle traces over a NACA 0012 airfoil oscillated in plunge at $k = 0.8$ and $h_0 = 0.50$.

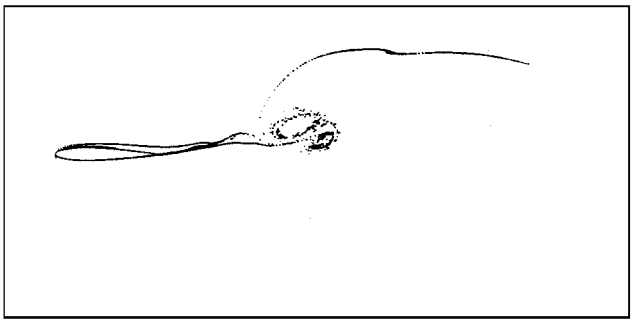

h = 0.07

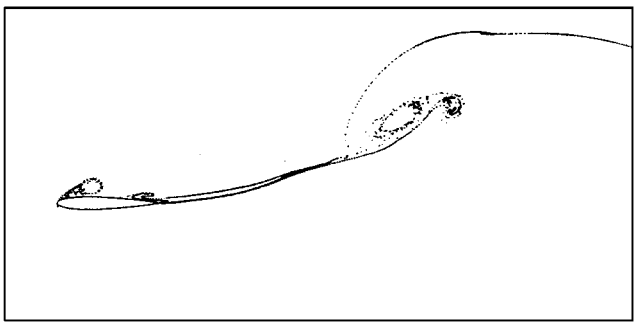

h = −0.37

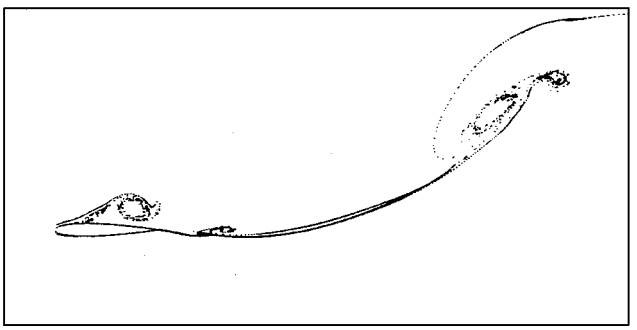

h = −0.59

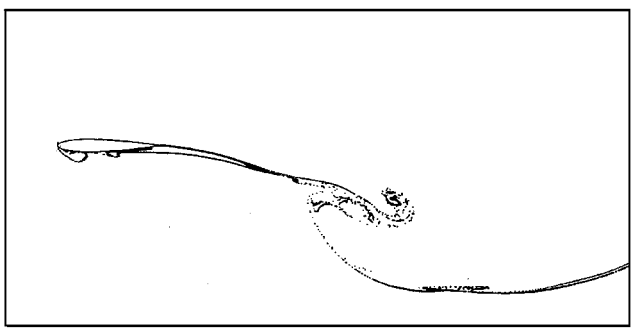

h = 0.19

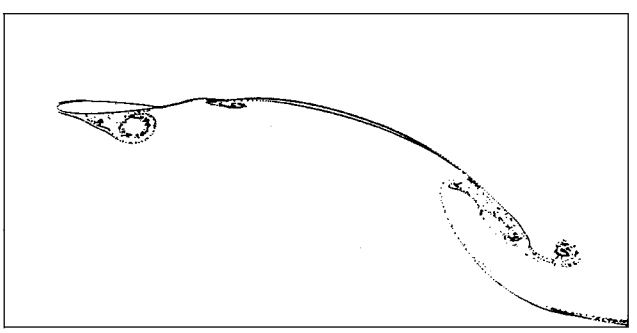

h = 0.59

Fig. 4c Unsteady particle traces over a NACA 0012 airfoil oscillated in plunge at $k = 0.8$ and $h_0 = 0.60$.

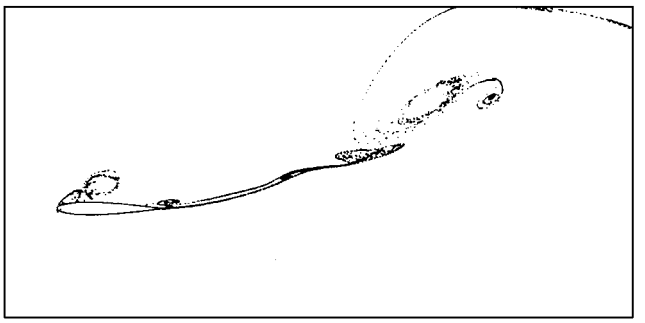

h = −0.44

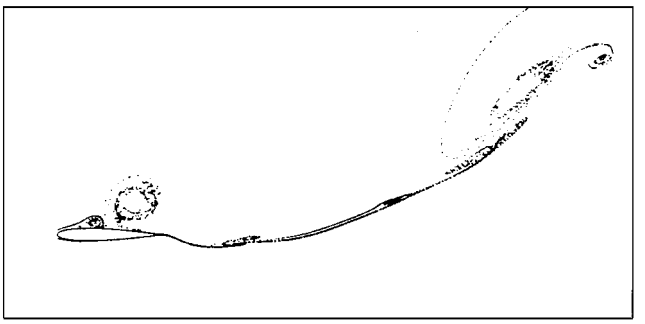

h = −0.69

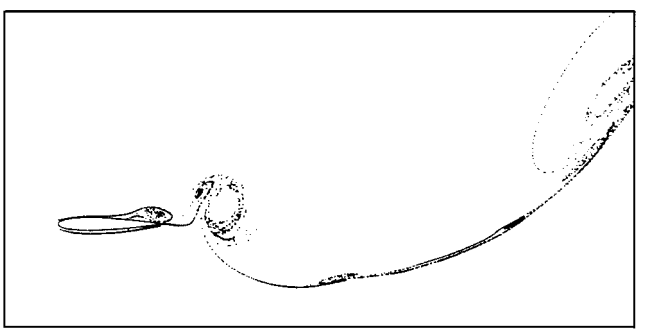

h = −0.52

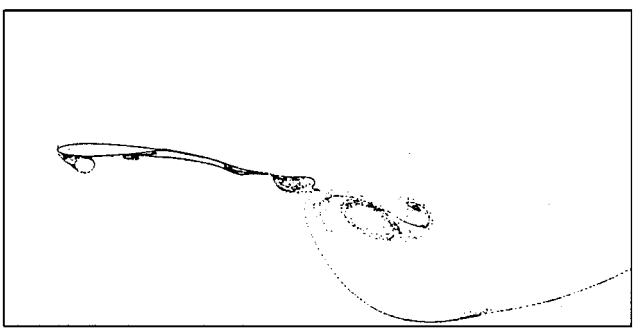

h = 0.16

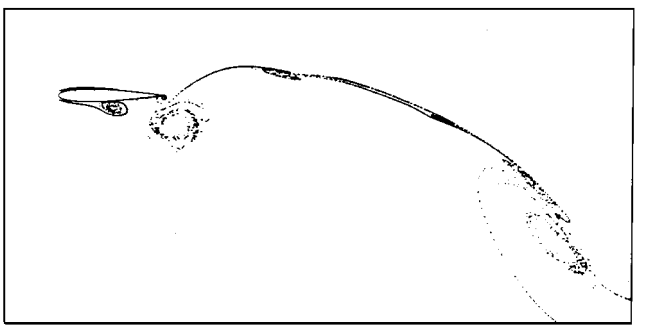

h = 0.67

Fig. 4d Unsteady particle traces over a NACA 0012 airfoil oscillated in plunge at $k = 0.8$ and $h_0 = 0.70$.

Table 2 Thrust of efficiency of NACA 0012 airfoil oscillated in plunge

$k = 0.8$		
h_0	$\bar{C}_D$	η
0.40	−0.118	**0.59**
0.50	**−0.176**	0.55
0.60	−0.134	0.28
0.70	−0.123	0.17

Table 3 Thrust and efficiency of NACA 0012 airfoil oscillated in combined plunge and pitch

$h_0 = 1$, $\alpha_0 = 10$ deg			
k	ϕ	$\bar{C}_D$	η
0.3	90	−0.072	**0.86**
0.3	30	−0.116	0.70
1.0	90	**−0.446**	0.25
1.0	30	−0.211	0.11

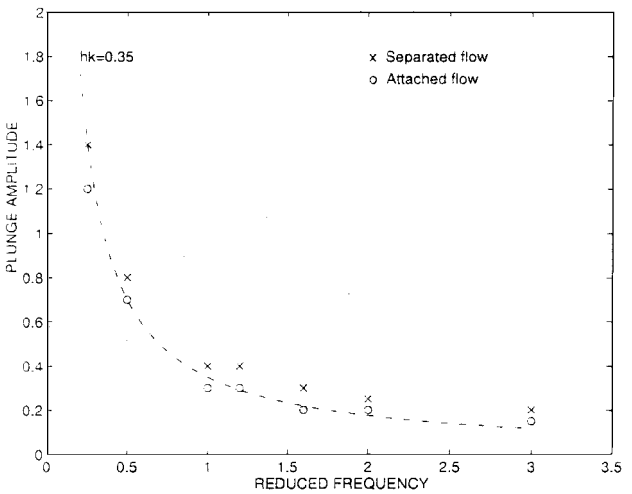

Fig. 5 Plunge amplitude vs reduced frequency at stall onset.

At $h_0 = 0.50$ small recirculating regions appear at the downstream half of the airfoil during the up- and downstrokes. The vortex is then shed into the wake. While preserving a high propulsive efficiency, it produces the largest thrust coefficient of 0.176. As the amplitude of the plunge motion increases up to 0.6 and 0.7 (Figs. 4c and 4d), the light flow separation at the leading edge turns into the formation of a large-scale dynamic stall vortex during both the up- and downstrokes. The dynamic stall vortex convects downstream and sheds into the wake. At $h_0 = 0.7$ secondary leading-edge vortices are also generated. The vortical flow structure, and therefore the mechanism of thrust generation, caused by the shedding of dynamic stall vortices from the airfoil leading edge is clearly quite different from the vortex street produced by vortices shed from the trailing edge only. Yet, as shown in Table 2, comparable thrust levels are maintained in this case, albeit at significantly reduced propulsive efficiencies. These results are consistent with the dynamic stall boundary of $h_0 k = 0.35$, which we identified in our earlier investigation.[9] This dynamic stall boundary is shown in Fig. 5.

We then computed the flowfields over an airfoil oscillated in a combined pitch-and-plunge motion at high amplitudes and low frequencies. The Reynolds number was again 1×10^5. Pitch oscillation is about the midchord and leads the plunge oscillation by a phase angle ϕ. Figures 6a–6d show the computed flowfields, and Table 3 gives the thrust coefficient and the propulsive efficiency of the airfoil. As observed again, the propulsive efficiency is much larger for the attached flow cases given in Figs. 6a and 6b. For the remaining cases, where a leading-edge vortex forms and the airfoil undergoes a dynamic stall loop, although the average thrust coefficient is higher, the efficiency again drops significantly. This trend can be attributed to the fact that additional work has to be done against the suction induced by the vortex. In addition, when the strong leading-edge vortex is shed into the wake, it disrupts the jet-like flow at the trailing edge.

Isogai et al.[10] compared their results with our computations (Figs. 17 and 18 of Ref. 10) and found fairly good agreement, except for phase angles of 30 deg, where they found severe leading-edge separation. This discrepancy requires further investigation.

Finally, we computed some flowfields whose conditions were close to the ones studied recently by Anderson et al.[12] through flow visualization and force measurements at low Reynolds numbers (1.1×10^3). In the experiments the airfoil was pitched about the one-third chord point at various phase angles, and a digital particle image velocimetry was used to obtain visualization data. They associated high propulsive efficiency with moderately strong leading-edge vortices convecting downstream. They also found that the combined pitch-and-plunge motion at $\phi = 75$ deg, $h_0 = 0.75$, $\alpha_0 = 30$ deg, $k = 1.34$ is optimal for propulsive efficiency. The average thrust coefficient for this case, which is computed by integrating the excess velocity in the wake, is reported to be 0.34 (Table 2 of Ref. 12). It is equivalent to 0.20 if it is normalized with the chord only, which is how it is defined in our study, instead of the airfoil surface area. The propulsive efficiency is reported to be above 80%.

The flowfield matrix we were able to compute is given in Table 4. The flowfields were computed at $Re = 1 \times 10^4$ again assuming fully turbulent flow. We could not compute at higher pitch amplitudes for the given reduced frequencies because of convergence difficulties of the solver. However, the observation is made that at $k = 1$

Table 4 Thrust and efficiency of NACA 0012 airfoil oscillated in combined plunge and pitch

$h_0 = 0.75$, $\phi = 75$ deg			
k	α_0	$\bar{C}_D$	η
1.0	7	−0.29	0.29
1.0	15	−0.31	0.54
1.0	20	−0.177	**0.56**
1.34	7	−0.371	0.20
1.34	10	**−0.446**	0.26

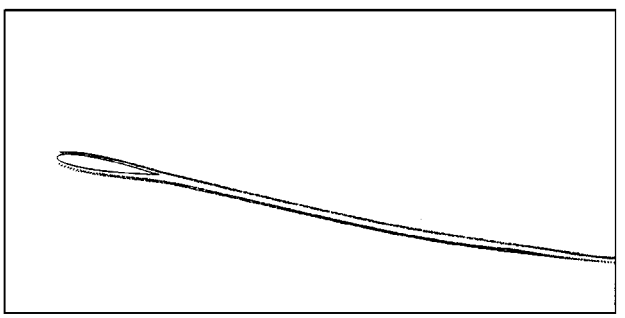

Fig. 6a Unsteady particle traces over a NACA 0012 airfoil oscillated in pitch and plunge at $k = 0.3$, $\phi = 90$ deg, $\alpha_0 = 10$ deg, and $h_0 = 1$.

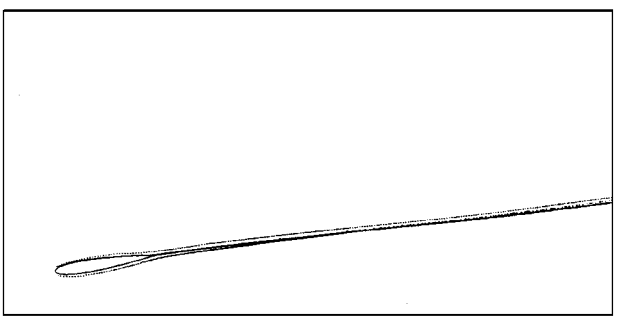

Fig. 6b Unsteady particle traces over a NACA 0012 airfoil oscillated in pitch and plunge at $k = 0.3$, $\phi = 30$ deg, $\alpha_0 = 10$ deg, and $h_0 = 1$.

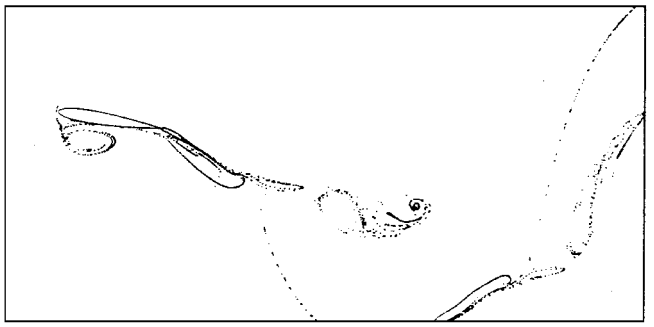

h = 0.41 α = 9.11

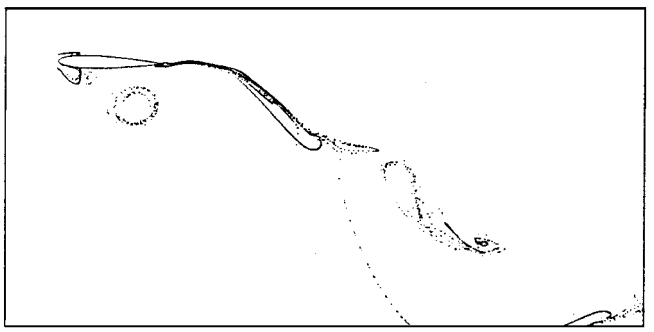

h = 0.98 α = 1.45

h = 0.79 α = −6.01

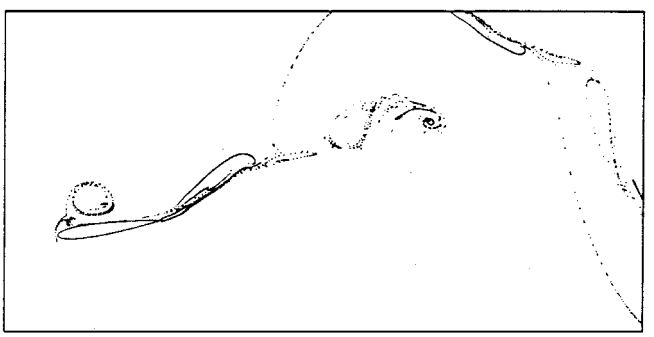

h = −0.53 α = −8.47

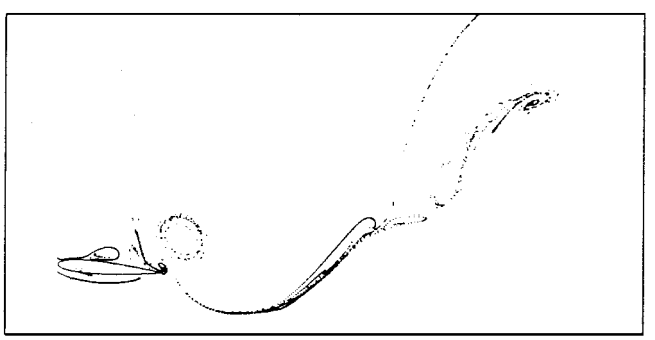

h = −0.88 α = 4.72

Fig. 6c Unsteady particle traces over a NACA 0012 airfoil oscillated in pitch and plunge at $k = 1$, $\phi = 90$ deg, $\alpha_0 = 10$ deg, and $h_0 = 1$.

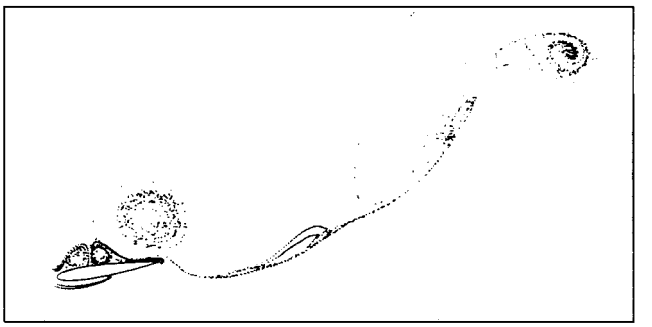

h = −0.99 α = −8.59

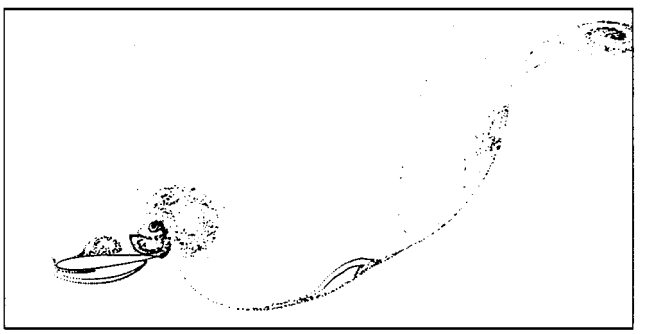

h = −0.87 α = −5.08

h = −0.05 α = 4.5

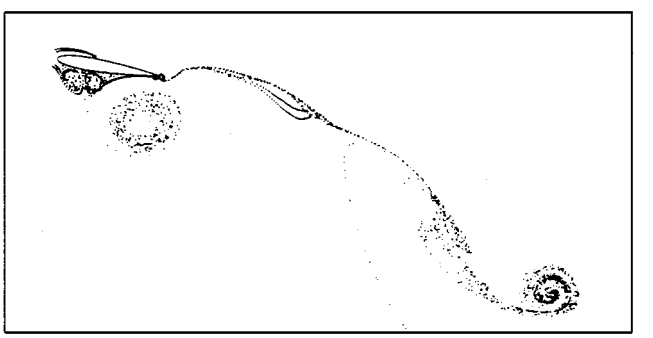

h = 0.99 α = 9.21

h = 0.19 α = −3.22

Fig. 6d Unsteady particle traces over a NACA 0012 airfoil oscillated in pitch and plunge at $k = 1$, $\phi = 30$ deg, $\alpha_0 = 10$ deg, and $h_0 = 1$.

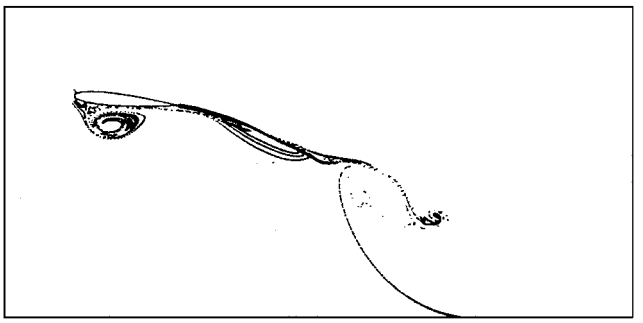

h = 0.6 α = 5.42

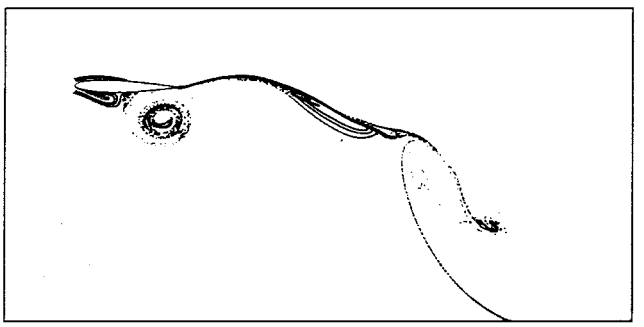

h = 0.74 α = 0.94

Fig. 7a Unsteady particle traces over a NACA 0012 airfoil oscillated in pitch and plunge at $\alpha_0 = 7$ deg, $h_0 = 0.75$, $k = 1$, and $\phi = 75$ deg.

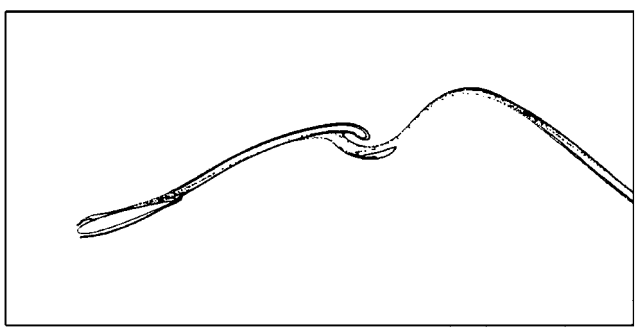

h = −0.5 α = −17.75

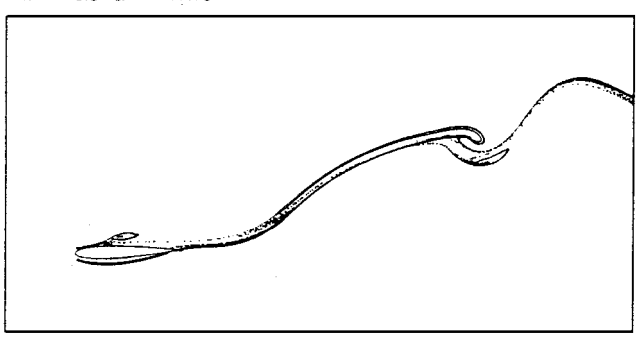

h = −0.73 α = −1.83

Fig. 7b Unsteady particle traces over a NACA 0012 airfoil oscillated in pitch and plunge at $\alpha_0 = 20$ deg, $h_0 = 0.75$, $k = 1$, and $\phi = 75$ deg.

the propulsive efficiency increases with increasing α_0. The computed flowfields at $k = 1$ are given for $\alpha_0 = 7$ and 20 deg in Fig. 7. As α_0 increases, the massive flow separation caused by a large leading-edge vortex disappears, and the flow stays mostly attached over the upper and lower surfaces. For $k = 1$, $\alpha_0 = 20$ deg, the thrust coefficient is computed to be 0.177.

Conclusions

Particle traces integrated into a thin-layer Navier–Stokes solver were obtained over a NACA 0012 airfoil oscillating in either pure plunge or a combined pitch-and-plungemotion. Particle traces captured the flow separation characteristics and wake profiles remarkably well. The computed wake profiles were found to be in good agreement with the water-tunnel experiments. The observation was made that higher propulsive efficiencies are associated with attached flows over the full period of the oscillatory cycle. At high-frequency plunging motions, in the presence of large leading-edge vortices, higher thrust coefficients can be obtained, but the propulsive efficiency drops significantly. In combined pitch-and-plunge oscillations it appears that high thrust values with reasonably high propulsive efficiency can be obtained under certain conditions. Further studies are needed to explore the combined pitch-and-plunge oscillations at high angles of attack.

Acknowledgment

The authors gratefully acknowledge the partial support of this investigation by the Naval Research Laboratory (project monitor Kevin Ailinger).

References

[1] Carr, L. W., and Chandrasekhara, M. S., "Compressibility Effects on Dynamic Stall," *Progress in Aerospace Sciences*, Vol. 32, No. 6, 1996, pp. 523–573.

[2] Ekaterinaris, J. A., and Platzer, M. F., "Computational Prediction of Airfoil Dynamic Stall," *Progress in Aerospace Sciences*, Vol. 33, No. 11/12, 1977, pp. 759–846.

[3] Garrick, I. E., "Propulsion of a Flapping and Oscillating Airfoil," NACA TR-567, May 1936.

[4] Platzer, M. F., Neace, K. S., and Pang, C. K., "Aerodynamic Analysis of Flapping Wing Propulsion," AIAA Paper 93-0484, Jan. 1993.

[5] Jones, K. D., Dohring, C. M., and Platzer, M. F., "Experimental and Computational Investigation of the Knoller–Betz Effect," *AIAA Journal*, Vol. 36, No. 7, 1998, pp. 1240–1246.

[6] Lai, J. C. S., and Platzer, M. F., "Jet Characteristics of a Plunging Airfoil," *AIAA Journal*, Vol. 37, No. 12, 1999, pp. 1529–1537.

[7] Tuncer, I. H., and Platzer, M. F., "Thrust Generation Due to Airfoil Flapping," *AIAA Journal*, Vol. 34, No. 2, 1995, pp. 324–331.

[8] Tuncer, I. H., Lai, J., Ortiz, M. A., and Platzer, M. F., "Unsteady Aerodynamics of Stationary/Flapping Airfoil Combination in Tandem," AIAA Paper 97-0659, Jan. 1997.

[9] Tuncer, I. H., Walz, R., and Platzer, M. F., "A Computational Study on the Dynamic Stall of a Flapping Airfoil," AIAA Paper 98-2519, June 1998.

[10] Isogai, K., Shinmoto, Y., and Watanabe, Y., "Effects of Dynamic Stall on Propulsive Efficiency and Thrust of Flapping Airfoil," *AIAA Journal*, Vol. 37, No. 10, 1999, pp. 1145–1151.

[11] Ramamurti, R., Sandberg, W., and Loehner, R., "Simulation of Flow About Flapping Airfoils Using a Finite Element Incompressible Flow Solver," AIAA Paper 99-0652, Jan. 1999.

[12] Anderson, J. M., Streitlien, K., Barrett, D. S., and Triantafyllou, M. S., "Oscillating Foils of High Propulsive Efficiency," *Journal of Fluid Mechanics*, Vol. 360, April 1998, pp. 41–72.

[13] Rai, M. M., and Chakravarthy, S. R., "An Implicit Form of the Osher Upwind Scheme," *AIAA Journal*, Vol. 24, No. 5, 1986, pp. 735–743.

[14] Tuncer, I. H., "A Particle Tracing Method for 2-D Unsteady Flows on Curvilinear Grids," American Society of Mechanical Engineers, Paper FEDSM97-3071, June 1997.